

# Impact of laser-enhanced contact optimization on n-TOPCon solar cells' performance and efficiency: Experimental and simulated insights

Qinqin Wang<sup>a,\*</sup>, Kaiyuan Guo<sup>a</sup>, Siwen Gu<sup>b</sup>, Wangping Wu<sup>b</sup>, Lvzhou Li<sup>a</sup>, Deniz Eren Erişen<sup>c</sup>, Gao Yong<sup>d</sup>, Jianning Ding<sup>a,\*\*</sup>

<sup>a</sup> Institute of Technology for Carbon Neutralization, Yangzhou University, Yangzhou, 225009, China

<sup>b</sup> Jiangsu Collaborative Innovation Center of Photovoltaic Science and Engineering, Changzhou University, Changzhou, 213164, China

<sup>c</sup> College of Material Science and Technology, Nanjing University of Aeronautics and Astronautics, Nanjing, Jiangsu, China

<sup>d</sup> Yingkou Jinchen Machinery Co., Ltd, China



## ARTICLE INFO

### Keywords:

Laser enhanced contact optimization  
TOPCon solar cell  
Sintering temperature  
Laser energy  
Reverse voltage  
COMSOL

## ABSTRACT

The laser-enhanced contact optimization (LECO) process, instead of the conventional high-temperature sintering process on the tunnel oxide passivated contact (TOPCon) solar cells, is being migrated to mainstream technology, with ongoing improvements in recent years. This study examines the impact of various process parameters—including sintering temperature, laser power, and reverse voltage—within the LECO process on the metallization-induced recombination current density associated with metal contact (denoted as  $J_{0,metal}$ ), contact resistivity (represented as  $\rho_c$ ), and current-voltage (I-V) characteristics. On the basis of the experiment, COMSOL simulations were introduced to model the changes in charge carrier dynamics during LECO. The influence of laser power and reverse voltage on the front surface electron concentration was systematically investigated and confirmed. The findings indicated that appropriately reducing the sintering temperature can significantly decrease metallization recombination. At the same time, the open-circuit voltage ( $V_{oc}$ ) showed a negative correlation with both the laser energy and reverse voltage. Conversely, the fill factor (FF) and contact resistivity ( $\rho_c$ ) positively correlated with these factors. Data from  $\rho_c$  and I-V measurements demonstrated that adequate laser energy is crucial for achieving sufficient carrier concentrations, which is necessary for minimizing  $\rho_c$ . However, excessively high laser energy may harm the passivation layer. Simulation analysis confirmed that the laser in the LECO process generates electron-hole pairs, while the reverse voltage separates the electrons and holes. We implemented the LECO process utilizing a sintering temperature of 790 °C, laser power of 18 W, and a reverse voltage of 16 V to enhance the maximum efficiency. ( $E_{ff}$ ) of 25.97 %, corresponding to a short-circuit current density ( $J_{sc}$ ) of 42.05 mA/cm<sup>2</sup>, a  $V_{oc}$  of 731.5 mV, and a fill factor (FF) of 84.42 %. The findings presented herein provide valuable insights that will inform the subsequent investigation of novel cell structures.

## 1. Introduction

In recent years, n-TOPCon solar cells have garnered considerable attention within the photovoltaic cells industry. The report anticipates that they may account for as much as 53 % of the market share by 2025 [1]. n-TOPCon solar cells stand out because they feature a unique ultrathin silicon oxide ( $SiO_x$ ) layer paired with n<sup>+</sup>-polycrystalline silicon (poly-Si). This layer is applied to the rear side, utilizing the excellent interface chemical passivation provided by  $SiO_x$  (usually measured at 1–2 nm), combined with the field-effect passivation of heavily doped

poly-Si layers [2,3]. This design helps to achieve a low recombination current density ( $J_0$ ) and reduced contact resistivity ( $\rho_c$ ) [4–8]. However, the conversion efficiency of these mass-production cells is limited to 25.8 %. This interesting phenomenon mainly happens because of carrier recombination between the front metal contact and the emitter, and it can significantly influence overall performance [9]. The laboratory efficiency of n-TOPCon solar cells has reached a remarkable level of 26.58 % [10]. Utilizing the laser-doping technique effectively minimizes contact recombination losses, leading to a significant boost in efficiency [11]. The n-TOPCon solar cell is engineered with two fundamental

\* Corresponding author.

\*\* Corresponding author.

E-mail addresses: [wangqinqin@yzu.edu.cn](mailto:wangqinqin@yzu.edu.cn) (Q. Wang), [dingjn@yzu.edu.cn](mailto:dingjn@yzu.edu.cn) (J. Ding).

layers, each playing a crucial role in its operational efficiency. The front side features a boron-doped p+ layer, which is characterized by a predominant presence of holes, acting as the majority carriers where holes represent the absence of electrons, facilitating the flow of electric current when the cell is engaged in energy conversion. Conversely, the rear side of the cell comprises a phosphorus-doped n-region. This layer is imperative as it provides the electrons essential for the oxidation-reduction reactions involving silver (Ag) at the cell's electrode. These electrochemical reactions are pivotal to the cell's efficiency. Nonetheless, a critical challenge arises from the interaction between these two layers. Efficient charge carrier transport necessitates electrons from the n-region to establish robust contact with the p-region. However, empirical observations indicate that inadequate contact often occurs at the interface between the p-region and n-region. Such insufficient connectivity can lead to performance inefficiencies, ultimately compromising the solar cell's effectiveness in capturing and converting solar energy into useable electrical power. Therefore, a comprehensive understanding of the interactions between these regions is essential for advancing solar cell technology and enhancing performance metrics [12]. To address this challenge, aluminum was added to the paste formulation, while the glass etching passivation layer was utilized to create conductive channels. This process results in the formation of silver-aluminum spikes, which enhance direct contact and significantly improve the electrical connection in the p+ region of the TOPCon cell [13]. However, this method inherently increases the metallization-induced recombination current density ( $J_{0,metal}$ ) on the p+ layer. The flow properties and characteristics of aluminum limit the silver-aluminum paste's ability to establish optimal contact in all etched areas after applying the passivation layer etching. This results in void formation, causing notable degradation of the passivation layer. These issues collectively led to a decrease in the open-circuit voltage ( $V_{oc}$ ) of the cell, while the  $J_{0,metal}$  on the front side remains high, approximately 400 fA/cm<sup>2</sup> [14]. In contrast, the  $J_{0,metal}$  on the rear side of the TOPCon structure is relatively lower, ranging from 50 to 100 fA/cm<sup>2</sup> [15].

There are two methods to minimize the metallization current density on the p+ region. The preliminary methodology entails the utilization of selective emitters (SE), comprising lightly doped emitters situated within the passivation region and highly doped emitters positioned beneath the metal contact. It can diminish the  $J_{0,metal}$  and  $\rho_c$ , and enhance FF and  $V_{oc}$ . At present, the  $J_{0,metal}$  can be reduced to 213 fA/cm<sup>2</sup> [9]. A widely used technique is laser doping, which promotes the movement of boron from Borosilicate Glass (BSG) into the lightly doped region, thereby establishing heavily doped regions. However, implementing laser doping requires a large amount of laser energy, and both excessive and insufficient energy can adversely affect the subsequent processing of the solar cell [15]. The second approach requires the preparation of a double-sided polycrystalline silicon cell featuring a positive p+-poly-Si layer. A major challenge associated with p+-poly-Si is its relatively low surface passivation capability, with  $J_0$  values exceeding 10 fA/cm<sup>2</sup> [16–23]. Furthermore, the compatibility of this material with metallization processes is constrained [24].

A novel sintering technology referred to as Laser Enhanced Contact Optimization (LECO) has been developed to mitigate recombination induced by metallization. The fundamental principle underlying LECO technology entails the utilization of continuous infrared laser irradiation on cells, consequently generating a substantial number of photo-generated charge carriers. At the same time, a reverse voltage of 10–20 V is used to guide the flow of charge carriers [25], ultimately promoting the optimization of contacts. This method produces a significant current via small contacts positioned at the apex of the cell pyramid [26], causing ignition at the corresponding positions and promoting the interdiffusion of the silver and silicon. This interaction significantly reduces the  $\rho_c$  between the metal and the semiconductor [27]. Initially, LECO technology was applied to repair cells with poor sintering, which was implemented in the passivated emitter and rear cell (PERC), resulting in an increase in  $V_{oc}$  by approximately 7 mV and an

**Table 1**  
Reviews on the research on the LECO process for solar cells.

Structure	Contact and passivation performance	I-V datas	Important results	Ref.
PERC	$\rho_c$ 1.3 mΩ cm <sup>2</sup>	$V_{oc}$ 675 mV, $J_{sc}$ 40.4 mA/cm <sup>2</sup> , FF 81.1 %	The LECO process improves the laser-fired monofacial cells with and without busbars to the performance level after conventional sintering.	[28]
PERC	/	$V_{oc}$ +6.9 mV, $J_{sc}$ +0.08 mA/cm <sup>2</sup> , FF +0.42 %, $E_{ff}$ +0.38 %	The efficiency gain of 0.38 %abs emphasize the great potential of the LECO process. Lowering the metallized fraction lowers the LECO gain.	[30]
TOPCon	/	$V_{oc}$ 711 mV, $J_{sc}$ 41.4 mA/cm <sup>2</sup> , FF 81.8 %, $E_{ff}$ 24.1 %	LECO allows for thinner and lower doped layers, and potentially the use of additional or thicker dielectric layers that are more resilient to penetration by metal pastes, a reduction of the metal area fraction and extended sintering or annealing conditions.	[24]
TOPCon	/	/	During the LECO process are in the order of several mA/cm <sup>2</sup> . Current densities decrease with increasing contact radii.	[26]
TOPCon	/	/	the LECO induced formation of an Ag <sub>x</sub> and Si <sub>y</sub> containing phase contacting the silver paste and the silicon (emitter). Silver was diffused into the silicon wafer (emitter) and silicon into the silver paste.	[27]
TOPCon	$\rho_c$ 0.9 mΩ cm <sup>2</sup> , $J_{0,metal}$ 206 fA/cm <sup>2</sup> , linear resistivity 2.6 μΩ cm	$V_{oc}$ 730.2 mV, $J_{sc}$ 42.02 mA/cm <sup>2</sup> , FF 84.39 %, $E_{ff}$ 25.94 %	Current collection is a mainly current tunneling through the glass layer, improving the glass passivation performance, resulting in the decrease in the metallization recombination and the increase in FF.	[29]

enhancement in fill factor (FF) by about 0.4 %, ultimately contributing to an overall efficiency increase of approximately 0.38 % [28]. Following the development of LECO-tailored pastes, this technology was swiftly implemented in the p+-region of n-TOPCon cells [30], which can lead to a decrease in  $J_{0,metal}$  [31]. Although the general principles of the LECO process have been discussed previously, as shown in Table 1, there has been no in-depth study on the influence of LECO process parameters on TOPCon solar cells. Therefore, this study focuses on the effects of LECO process parameters, including laser power, reverse voltage and sintering temperature, concerning their influences on  $\rho_c$ , the implied open circuit voltage (IV<sub>oc</sub>), the dark saturation current density, pseudo fill factor (pFF) and the I–V parameters of solar cells, i.e., efficiency ( $E_{ff}$ ), open-circuit voltage ( $V_{oc}$ ), short-circuit current ( $J_{sc}$ ), series resistance ( $R_s$ ), fill factor (FF). Although the heat produced during the LECO process has been simulated in earlier research [26], the crucial element of

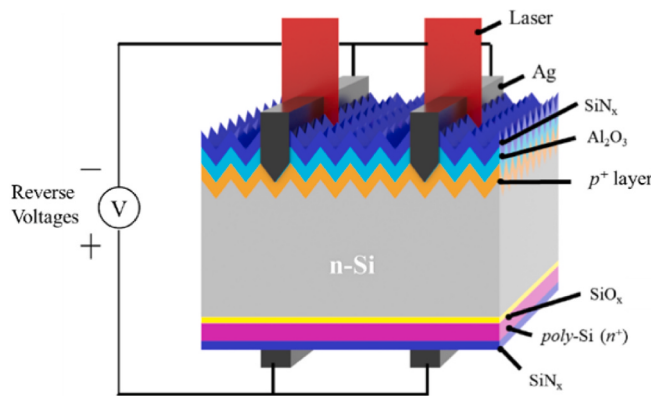


**Fig. 1.** n-TOPCon solar cell structure and LECO process.

carrier concentration variations under the combined impact of reverse voltage and laser has not been investigated. In order to clarify the implications of these parameters, we built a comprehensive model of a solar cell, simulated various laser power and reverse voltage circumstances, and compared the simulation findings with experimental measurements.

## 2. Materials and methods

A n-type industrial-grade TOPCon solar cell featuring 18 busbars was used, as shown in Fig. 1. The front side of the cell was boron (B) diffused emitter with sheet resistance of  $R_{\square,p+} = 230 \Omega/\text{sq}$ . The rear side structure was a  $\text{SiO}_x$  layer ( $1.4 \pm 0.2 \text{ nm}$ ) and a P-doped poly-Si ( $n^+$ -poly-Si) layer ( $100 \pm 20 \text{ nm}$ ).

Using atomic layer deposition (ALD), a 3 nm layer of  $\text{Al}_2\text{O}_3$  was deposited on the front side of the cell. Next, a passivation layer of 80 nm silicon nitride ( $\text{SiN}_x$ ) was deposited on both sides of the cell using the plasma-enhanced chemical vapor deposition (PECVD) method.

### 2.1. Printing and sintering of metallic paste

Metalization is accomplished by screen printing and sintering of both standard and LECO-tailored metallic pastes (TOPCon front LECO finger paste model RX2902, rear finger paste model RX2802C, bifacial busbar paste model RX2702) using an H-pattern grid design on both sides of the wafers. The sintering process was performed at varying peak sintering temperatures ( $760^\circ\text{C}$ ,  $790^\circ\text{C}$ , and  $820^\circ\text{C}$ ).

### 2.2. Laser-enhanced contact optimization

The front side was subjected to full-face laser scanning using an infrared laser ( $\lambda = 1064 \text{ nm}$ ,  $f = 200 \text{ kHz}$ , size =  $100 \mu\text{m} \times 100 \mu\text{m}$ ). The LECO process has been conducted at varying laser powers (18 W, 20 W, and 22 W) to investigate the effects of laser power. Additionally, the influence of different reverse voltages (15 V, 16 V, 17 V, and 18 V) and a constant power level (24 W) on the performance of n-TOPCon cells was assessed, ensuring compatibility with the LECO-tailored pastes.

### 2.3. Characterization

The microstructure of the cross-section of each finished cell, subjected to both conventional and LECO sintering, was characterized using Scanning Transmission Electron Microscopy (TEM, JEMF200). At the same time, the elemental composition was analyzed with an Energy Dispersive X-ray Spectroscopic (FESEM-EDS, Regulus8230).

The implied open circuit voltage ( $iV_{oc}$ ) values of the samples were

determined using the quasi-steady-state photoconductance (QSSPC) method (Transient Mode) under 1-sun illumination using a Sinton WCT-120 ( $@ 1 \times 10^{15} \text{ atoms}/\text{cm}^3$ ) lifetime tester.

The  $\rho_c$  samples were tested using the transfer-length-method (TLM-STD Millennial Solar, Suzhou, Jiangsu China). The dark saturation current density ( $J_{01}, J_{02}$ ) and pseudo fill factor ( $pFF$ ) values for the solar cells were tested using the Suns- $V_{oc}$  system (WCT-120 Sinton, Boulder, CO, USA).

The open-circuit voltage ( $V_{oc}$ ), short-circuit current ( $J_{sc}$ ), series resistance ( $R_s$ ), fill factor ( $FF$ ), and efficiency ( $E_{ff}$ ) of cells were measured by an  $I$ - $V$  tester under 1-sun illumination (AM 1.5).

## 2.4. Simulation

Simulations were conducted to model the concentrations of electrons and holes within the cell, aiming to investigate the roles of laser power and reverse voltage in the LECO process. The COMSOL Multiphysics simulation of semiconductors and electromagnetic waves is focused on, with particular attention being given to the interaction between these phenomena in the context of solar energy. A brief overview of the optical and electrical components involved is provided. The underlying physics of optical and electrical simulations has been extensively documented in the literature [32,33]. Additional formulations related to laser interactions are introduced, including the peak electric field  $E_0$ , the incident laser electric field  $E_{inc}$ , and the carrier generation rate  $G$ . These parameters are recognized as essential for understanding light absorption and carrier dynamics in semiconductor materials under solar irradiation.

$$E_0 = \left( \sqrt{\left( P_{ave} \times 8 \times n_0 \right) / \left( f_p \times D_x \times D_y \times D_t \right)} \right) \times \left( (-\log(0.5)/\pi)^{\frac{3}{4}} \right) \quad (1)$$

$$E_{inc} = E_0(x) \times e^{-\frac{4 \times \log(0.5) \times (x - x_0)^2}{D_y^2}} \quad (2)$$

$$G = alp / \left( f_0 \times h\_const \right) \times I \times e^{-\frac{-4 \times \log(2) \times (t - t_0)^2}{D_t^2}} \quad (3)$$

In this context,  $P_{ave}$  represents the average laser power,  $f_p$  is the laser repetition frequency,  $n_0$  is the vacuum characteristic impedance,  $D_x$  is the half-power width in the x-direction,  $D_y$  is the half-power width in the y-direction,  $D_t$  is the laser pulse width,  $x_0$  is the laser center position,  $t_0$  is the laser irradiation time,  $alp$  is the semiconductor extinction coefficient,  $f_0$  is the frequency, and  $h\_const$  is the Planck constant. The model consisted of a  $130 \mu\text{m}$  thick cell, with a bulk silicon phosphorus doping concentration of  $1.3 \times 10^{16} \text{ cm}^{-3}$  and a boron doping concentration of  $7 \times 10^{18} \text{ cm}^{-3}$  on the front surface, featuring a junction depth of  $0.6 \mu\text{m}$ .

The variation of electron and hole concentrations at the front surface was first simulated under different reverse voltages (0 V, 4 V, 8 V, 12 V, 16 V). Examining the changes in the curves, the electron and hole concentrations are primarily concentrated within the  $0\text{--}2.5 \mu\text{m}$  range on the front surface of the cell. For the laser simulation, we modeled a silicon substrate with a thickness of  $2.5 \mu\text{m}$ , maintaining the phosphorus doping concentration at  $1.3 \times 10^{16} \text{ cm}^{-3}$  and excluding boron doping on the front surface.

## 3. Results and discussion

The cells processed with normal sintering exhibited significant damage at the tips of the pyramids on the front surface, with distinct corrosion pits observed, as shown in Fig. 2(a). In contrast, the LECO-treated sample, which utilized aluminum-free silver paste for printing the gridlines, displayed no visible corrosion on the pyramids. It revealed the presence of a distinct glass layer that facilitates current tunneling and found large quantities of silver colloids in it, as illustrated in Fig. 2

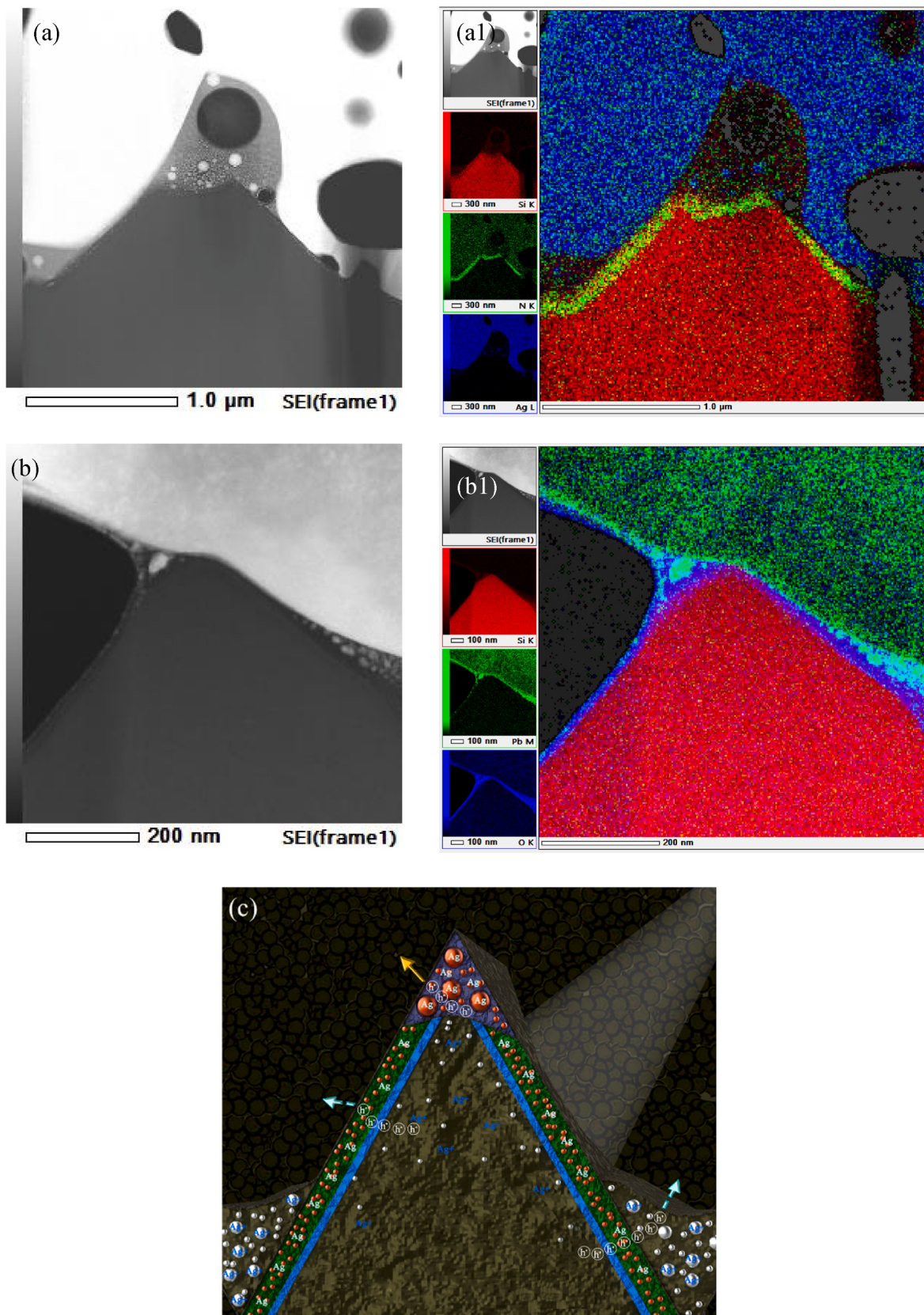


**Fig. 2.** STEM images of Ag-Si contact structure on (a) normal sintering cell, EDX image was observed in (a1); (b) LECO sintering cell, EDX image was observed in (b1); (c) current transport model of LECO [29].

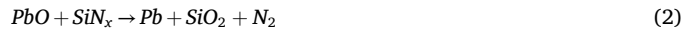
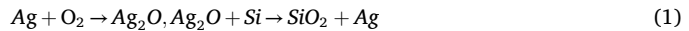
**Table 2**

Detailed I-V data for different sintering temperatures.

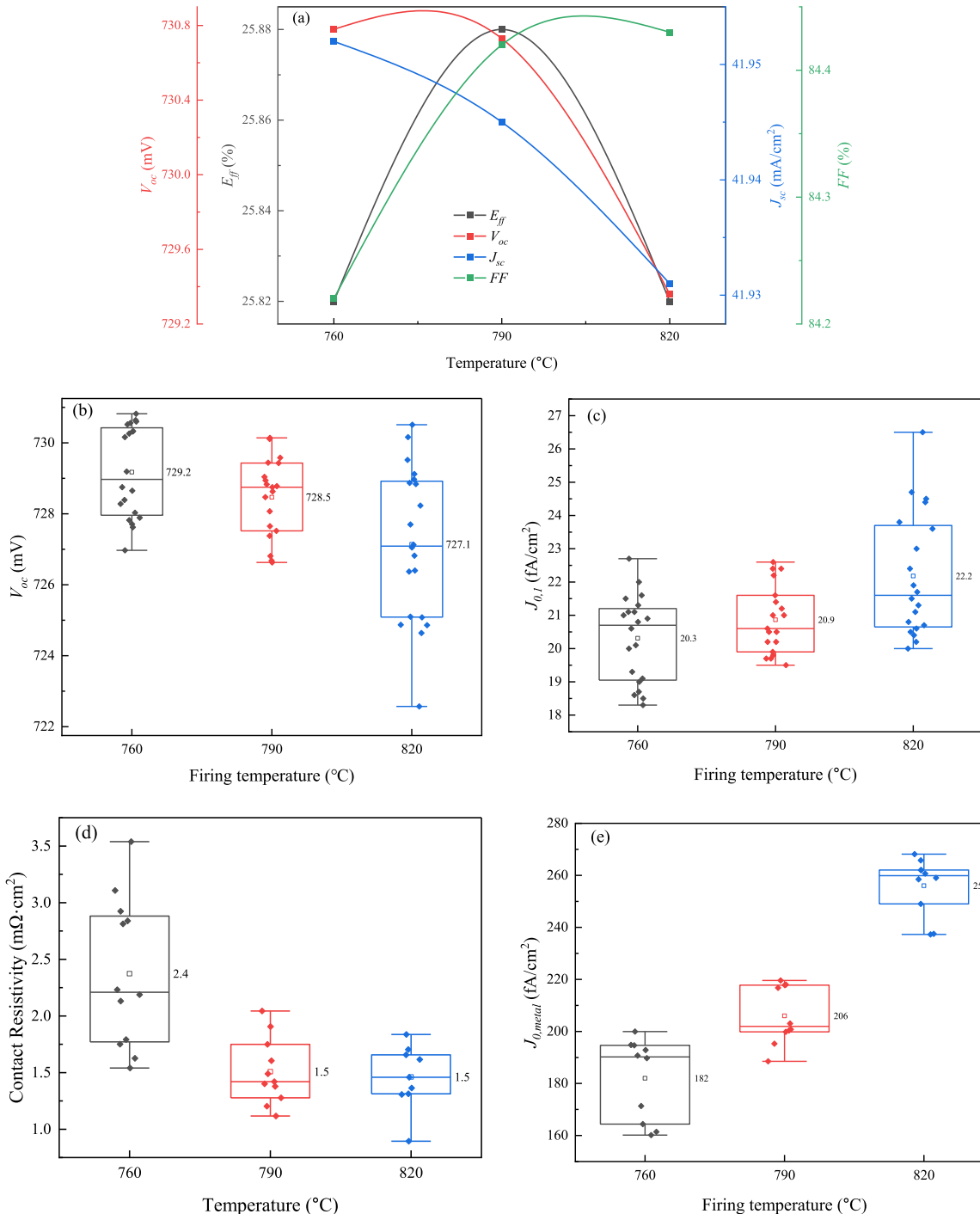
sintering temperature (°C)	$E_{ff}$ (%)	$V_{oc}$ (mV)	$J_{sc}$ (mA/cm <sup>2</sup> )	FF (%)	Cell area (cm <sup>2</sup> )
BL	25.61	727.1	41.85	84.16	334.71
760	25.82	730.7	41.95	84.22	
790	25.88	730.7	41.94	84.42	
820	25.82	729.3	41.93	84.43	

(b).

Previous studies on current transport pathways during LECO treatment have been extensively investigated, resulting in a schematic diagram illustrating the current tunneling transport in the LECO sample, as shown in Fig. 2(c). The reaction equation for Ag colloid formation is:



In equation (1), Ag undergoes a redox reaction and dissolves into the glass. In equation (2), the Pb lowers the Ag-Si interaction temperature, when cooled, the molten system Ag is deposited on the Si surface and

**Fig. 3.** (a) I-V data, (b)  $V_{oc}$  from Suns- $V_{oc}$ , (c)  $J_{0,1}$  and (d)  $\rho_c$  and (e)  $J_{0,metal}$  for cells at different sintering temperatures.

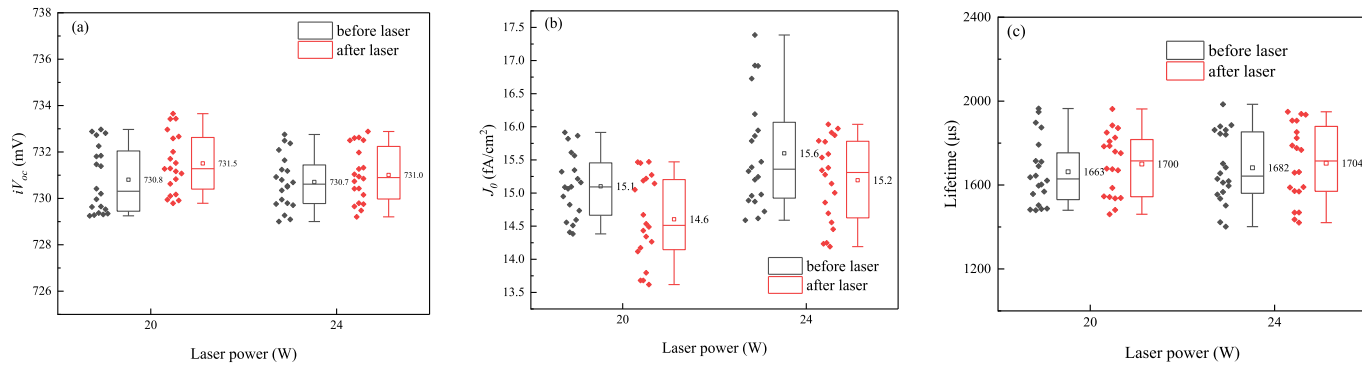


**Fig. 4.** (a)  $iV_{oc}$ , (b)  $J_0$  and (c) Lifetime before and after laser irradiation.

within the glass layer. In the LECO process, current transmission occurs through two primary mechanisms: (1) Direct Transmission via Silver-Silicon Contact: Dissolved  $\text{Ag}^+$  ions are transported through the molten glass layer to the emitter surface. Upon reaching the silicon surface, they undergo an electrochemical redox reaction, depositing as Ag crystallites. This forms a direct silver-silicon contact at the top of the pyramid, enabling the hole current ( $\text{h}^+$ ) to flow directly through this interface. (2) Tunneling through Metal Precipitates in the Glass Layer: During the cool-down phase, the molten glass layer becomes supersaturated with  $\text{Ag}^+$  ions, leading to the precipitation of Ag colloids within the interfacial glass layer. These localized Ag-rich regions form a network of nano-silver colloids interconnected by the silver finger. The hole current ( $\text{h}^+$ ) primarily flows through these metal precipitates via the tunneling effect (indicated by the dotted arrow). This mechanism enhances the passivation performance of the glass layer at the contact interface.

### 3.1. Influence of sintering temperature on contact

LECO (laser enhanced contact optimization), the main process is: 1) When printing the front grid line, the use of pure silver paste, due to the special treatment of the paste, reduce the corrosion capacity of the glass material, so the damage to the passivation layer is low; 2) rapid sintering at a lower temperature, further reduce the damage to the passivation layer; 3) laser and reverse voltage for secondary phase secondary sintering, to complete the silver silicon mutual diffusion, so as to optimize the contact. To achieve this performance during high-temperature sintering, it is essential to lower the sintering temperature. To confirm the effect of LECO process, we added a baseline group (BL) to the sintering temperature experiment. BL paste uses silver powder containing 2.1 % aluminum, and 90 % of the glass frit is Pb; LECO paste uses sterling silver powder, and the Pb content is reduced to 60 %. The initial sintering temperature was set at 820 °C (same as the BL), followed by reductions to 790 °C and 760 °C. Then the experimental group was subjected to LECO treatment (20V reverse voltage, 18W power laser irradiation). The I-V characteristics were evaluated, and the results are summarized in Table 2. The efficiency of the BL group is 0.26 % lower, primarily due to a 3.6 mV decrease in  $V_{oc}$  and a 0.26 % reduction in FF. This is attributed to the reduced damage of the paste to the passivation layer and the

enhanced contact performance resulting from the silver-silicon contact formed by diffusion. Additionally, the current is 0.09 mA/cm<sup>2</sup> lower, mainly because of the reduced line width. The highest efficiency was recorded at 790 °C, with a 1.4 mV higher  $V_{oc}$  compared to 820 °C, and a 0.2 % higher FF than at 760 °C. These data suggest that optimizing the sintering temperature involves balancing  $V_{oc}$  and FF, minimizing corrosion of the passivation layer, and enhancing contact quality. The results indicate that both  $\rho_c$  and  $V_{oc}$  increase with decreasing sintering temperature, as shown in Fig. 3. This observation supports the hypothesis that lowering the sintering temperature reduces corrosion of the passivation layer, albeit at the expense of contact performance. Furthermore, the  $J_{01}$  increases with higher sintering temperatures, suggesting that elevated sintering temperatures enhance interfacial recombination, which may contribute to the observed decrease in  $V_{oc}$ . At 760 °C,  $\rho_c$  shows a marked difference compared to 790 °C and 820 °C, indicating insufficient corrosion of the  $\text{SiN}_x$  layer by the glass in the paste. Consequently, the reduced silver particle density at the pyramid tips may hinder the formation of an optimal contact. The metal saturation current density ( $J_{0,\text{metal}}$ ) was calculated according to Equation (1):

$$J_{0,1} = [(1 - f_{\text{metal}}) * J_{0,\text{pass}} + f_{\text{metal}} * J_{0,\text{metal}}] (\text{front}) + J_{0,\text{bulk}} \\ + [(1 - f_{\text{metal}}) * J_{0,\text{pass}} + f_{\text{metal}} * J_{0,\text{metal}}] (\text{rear}) \quad (1)$$

In the equation,  $J_{01}$  means junction region recombination current density,  $J_{0,\text{pass}}$  represents the recombination current within the passivation region,  $f_{\text{metal}}$  indicates the fraction of the metallization area,  $J_{0,\text{metal}}$  corresponds to the recombination associated with metallization, and  $J_{0,\text{bulk}}$  refers to recombination in the bulk. The findings on metallization recombination at different sintering temperatures are shown in Fig. 3(e). At 820 °C,  $J_{0,\text{metal}}$  was 256 fA/cm<sup>2</sup>. A decrease in sintering temperature to 790 °C and 760 °C resulted in a reduction of  $J_{0,\text{metal}}$  by approximately 200 fA/cm<sup>2</sup>. This suggests that lowering the sintering temperature reduces glass corrosion on the passivation layer, thereby enhancing the protective properties of the passivation layer for the metallization area. Furthermore, the impact of further temperature reduction on mitigating glass corrosion becomes less pronounced, with the remaining metallization composite primarily originating from silver-silicon interdiffusion induced by high currents generated during the induction process. The I-V data showed minimal variations at different sintering temperatures, indicating that although changes in sintering temperature affect the formation of contacts within the paste, the contacts formed through the LECO process predominantly rely on the tunneling action of silver colloids within the glass layer for current collection. Therefore, sintering temperatures within the range of 760 °C–820 °C have minimal impact on the electrical properties.

### 3.2. Influence of LECO process on n-TOPCon solar cell

#### 3.2.1. The laser power

The effects of laser power on the textured surface were investigated,

**Table 3**  
Detailed I-V data at different laser power.

Laser power (W)	$E_{ff}$ (%)	$V_{oc}$ (mV)	$J_{sc}$ (mA/cm <sup>2</sup> )	FF (%)	Cell area (cm <sup>2</sup> )
0	5.51	732.3	3.75	20.07	334.71
18	25.83	727.5	42.04	84.44	
20	25.82	726.9	42.04	84.47	
22	25.79	726.0	42.02	84.53	
24	25.44	718.7	41.87	84.53	

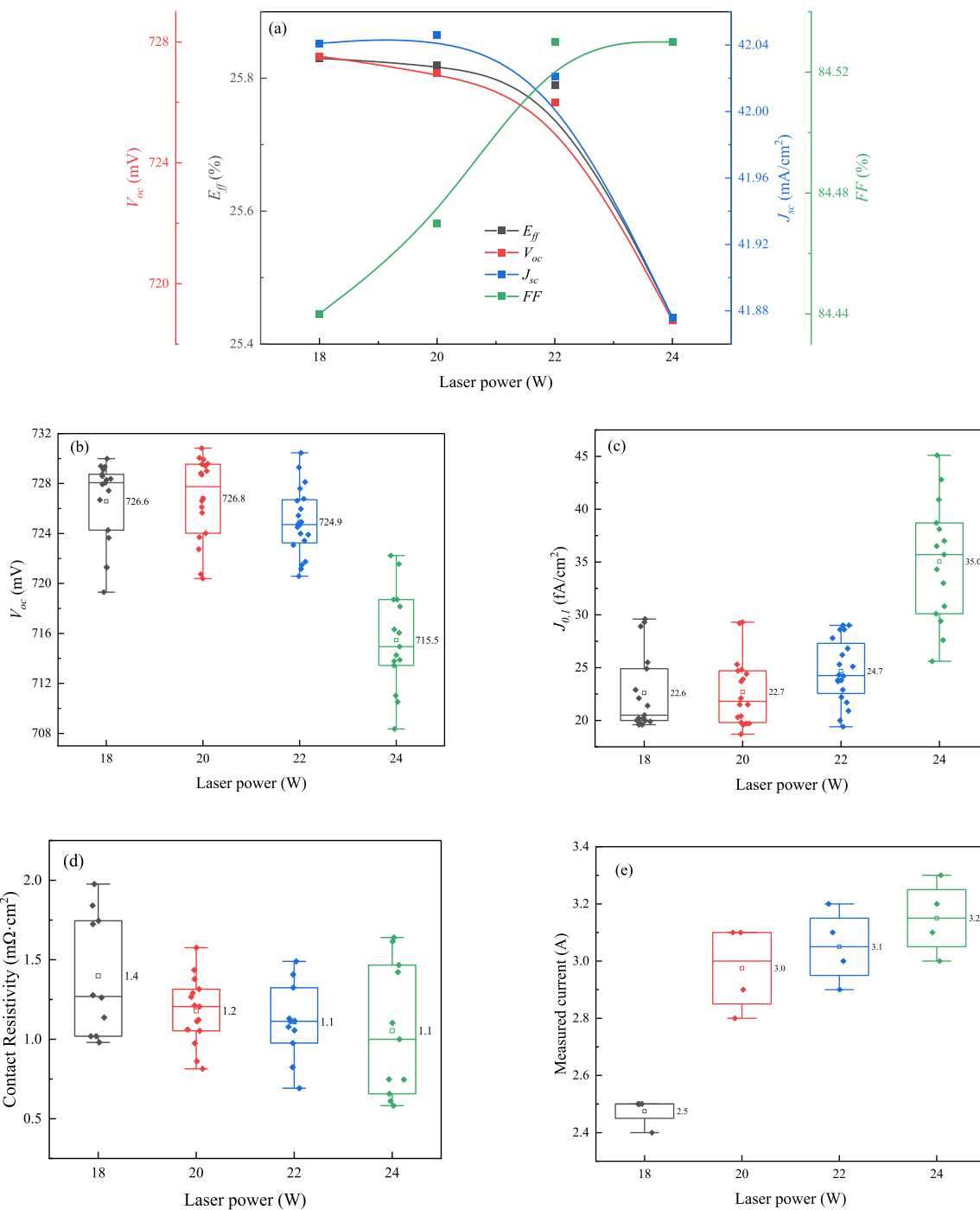


**Fig. 5.** (a)  $I$ - $V$  data, (b)  $V_{oc}$ , (c)  $J_{0,I}$ , (d)  $\rho_c$  and (e) measured current at different laser power.

as shown in Fig. S1. A comparative analysis of textured surfaces subjected to three different laser power levels revealed no significant changes, suggesting that direct laser irradiation does not cause substantial damage to the cells. To further validate this observation, a semi-finished product was subjected to laser irradiation, as depicted in Fig. 4. Remarkably, the minority carrier lifetime, implied open-circuit voltage ( $iV_{oc}$ ), and recombination current density ( $J_0$ ) exhibited significant improvements following laser treatment. These results indicate that laser irradiation activates a considerable number of previously inactive carriers, thereby increasing the minority carrier concentration and enhancing the minority carrier lifetime within the cell.

The  $I$ - $V$  characteristics of n-TOPCon cells are summarized in Table 3,

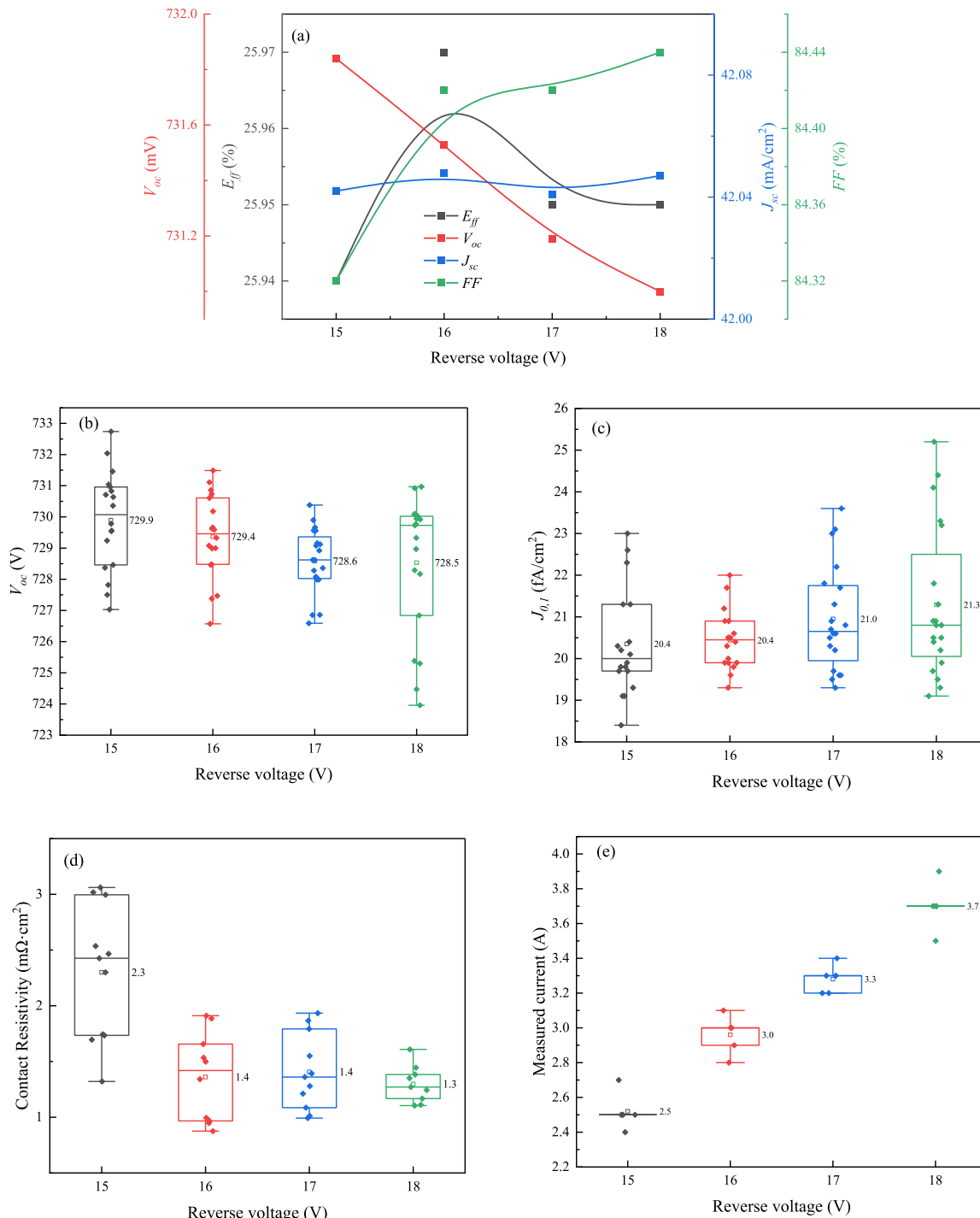
with the corresponding trend illustrated in Fig. 5(a). When the laser was not applied, the solar cell cannot form effective contact, resulting in extremely low FF. The maximum cell efficiency was achieved at laser powers of 18 W and 20 W. At laser powers below 22 W, the open-circuit voltage ( $V_{oc}$ ) exhibited minimal variation, decreasing by only 1 mV. This minor decrease is attributed to degradation of the surface passivation layer during the LECO process. However, increasing the laser power to 24 W caused an 8 mV reduction in  $V_{oc}$ , while the FF remained unchanged. Previous SEM analyses confirmed that laser treatment does not directly degrade cell performance, indicating that the  $V_{oc}$  reduction is not due to damage to the passivation layer. As shown in Fig. 5,  $Suns$ - $V_{oc}$  measurements revealed a significant increase in  $J_{0,I}$  at 24 W laser power,

**Table 4**

Detailed I-V data under different reverse voltages.

Reverse voltage (V)	$E_{ff}$ (%)	$V_{oc}$ (mV)	$J_{sc}$ (mA/cm <sup>2</sup> )	FF (%)	Cell area (cm <sup>2</sup> )
0	5.69	731.4	3.85	20.19	334.71
15	25.94	731.8	42.04	84.32	
16	25.97	731.5	42.05	84.42	
17	25.95	731.2	42.04	84.42	
18	25.95	731.0	42.05	84.44	

attributed to enhanced recombination at the metallized grid-line after laser treatment. This behavior likely arises because higher laser power generates more charge carriers, increasing current during the LECO process. The elevated current intensifies damage at the pyramid tips, enlarging the direct contact area between silver and silicon, and thereby increasing  $J_{0,metal}$ , contributing to the observed  $V_{oc}$  reduction. Fig. 5(d) shows that  $\rho_c$  decreased from 1.4 mΩ cm<sup>2</sup> to 1.1 mΩ cm<sup>2</sup> as laser power increased from 18 W to 22 W. Simultaneously, FF exhibited an upward trend, indicating improved contact quality with increasing laser power during the LECO process. However, this improvement in contact quality does not fully compensate for the damage in the metallized region,

**Fig. 6.** (a) I-V data, (b)  $V_{oc}$ , (c)  $J_{0,l}$ , (d)  $\rho_c$  and (e) measured current at different reverse voltages.

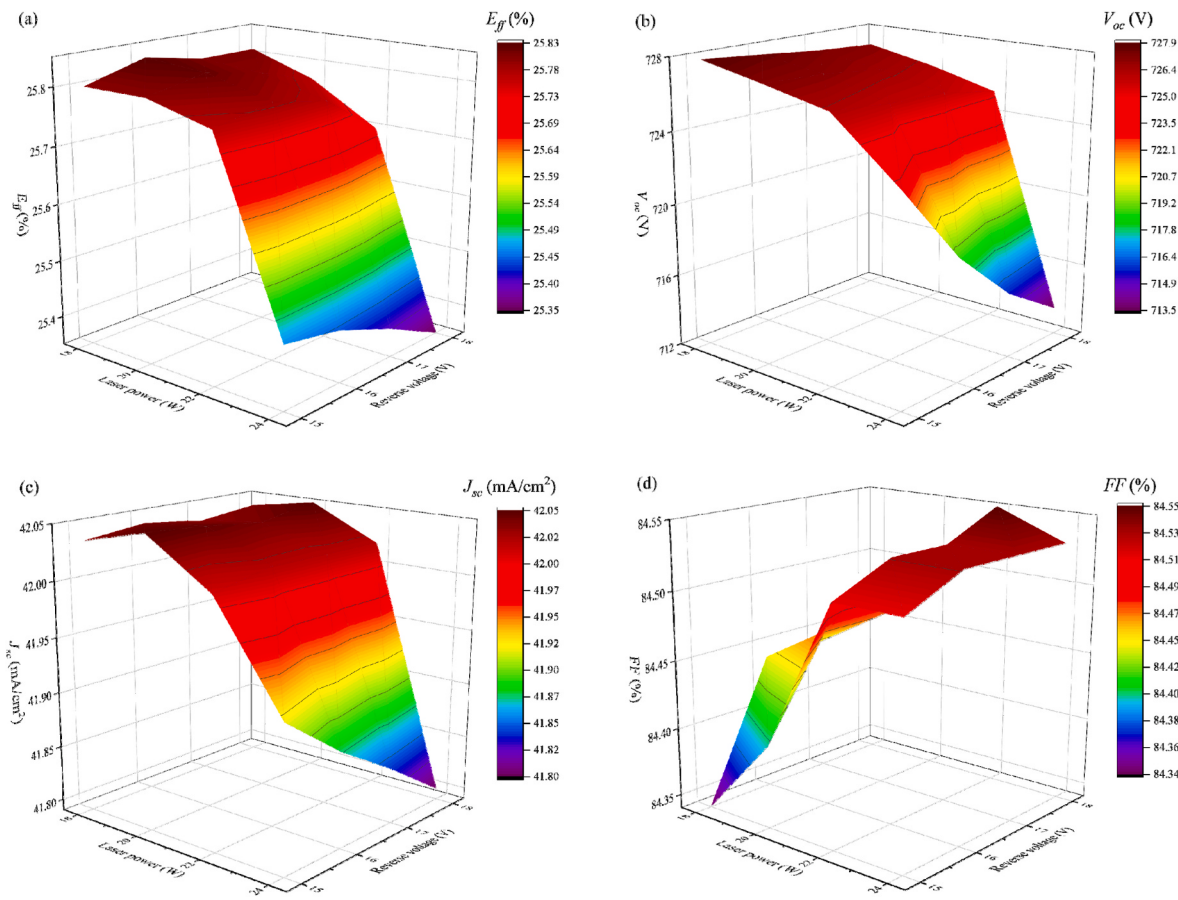


**Fig. 7.** (a)  $E_{ff}$ , (b)  $V_{oc}$ , (c)  $J_{sc}$  and (d) FF, as a function of the laser power and the reverse voltage of LECO process.

leading to a decrease in  $E_{ff}$ . These findings demonstrate that laser power significantly affects  $V_{oc}$  during the LECO process due to complex recombination effects in the metallized region. Furthermore, laser power influences FF by generating the necessary charge carriers for current collection. However, within a certain range, laser power has a limited effect on carrier excitation, resulting in minor changes in both FF and  $\rho_c$ . Current measurements during the LECO process revealed that at 18 W laser power, the current was 2.5 A, more than 0.5 A lower than at higher power levels, suggesting that reduced laser power limits charge carrier generation.

### 3.2.2. The reverse voltage

The reverse voltage in the LECO process plays a critical role by inducing reverse charge carrier movement during laser irradiation, thereby promoting current flow through regions with high contact resistance that have been slightly corroded by the paste. This process generates localized heating, which optimizes the contact. The I-V data are summarized in Table 4. When the reverse voltage was not applied, the solar cell also cannot form effective contact, just like when the laser is not applied, which proves that both laser and reverse voltage are indispensable in LECO process. Notably, an increase in reverse voltage results in a decrease in  $V_{oc}$  of approximately 1 mV, while the FF increases by 0.1 %. The short-circuit current density ( $J_{sc}$ ) remains unchanged. As laser energy increases, no significant degradation in electrical characteristics is observed, likely because the reverse voltage promotes directional charge carrier movement. Unless the voltage is insufficient to drive carriers into the contact region, its impact on contact formation is minimal. Electrical performance trends, presented in Fig. 6(a), indicate that a reverse voltage of 15 V results in a low FF. However, as the reverse voltage increases, FF rises to a plateau, consistent with theoretical expectations. This confirms the critical role of reverse voltage in the

process. *Suns-V<sub>oc</sub>* results (Fig. 6(b) and (c)) reveal minimal impact from reverse voltage variations; both  $V_{oc}$  and  $J_{sc}$  fluctuate only slightly, by 1 mV and 1 mA/cm<sup>2</sup>, respectively, demonstrating that reverse voltage has a negligible effect on cell performance. As shown in Fig. 6(d),  $\rho_c$  significantly decreases from 3.4 mΩ cm<sup>2</sup> to 1.3 mΩ cm<sup>2</sup> as the reverse voltage increases. However, once the voltage reaches 16 V,  $\rho_c$  plateaus, consistent with FF trends, suggesting that reverse voltage only needs to surpass a specific threshold to achieve optimal contact formation. Further increases yield diminishing returns. Based on contact resistivity and *Suns-V<sub>oc</sub>* results, the reverse voltage primarily affects contact formation in the LECO process, with minimal impact on  $V_{oc}$ . This is attributed to damage at the pyramid tips of the passivation layer in contact with the metal, leading to only minor changes in  $V_{oc}$ . Additionally, as shown in Fig. 6(e), the measured current increases with reverse voltage, supporting the observed reduction in contact resistivity.

The I-V data for cells subjected to varying reverse voltages and laser powers are presented as 3D plots in Fig. 7. Fig. 7(a) illustrates the relationship between  $E_{ff}$ , reverse voltage, and laser power. It is evident that laser power strongly influences cell efficiency, with trends in  $V_{oc}$  and  $J_{sc}$  mirroring those of efficiency. However, excessive laser power results in a rapid decline in efficiency. In contrast, the FF exhibits an upward trend with increasing reverse voltage and laser power. Once either parameter reaches a sufficiently high value, FF stabilizes within a higher range, suggesting that the enhancement of FF by the LECO process approaches its practical limit under these conditions.

### 3.3. COMSOL simulation

Results of different reverse voltage simulations, which show concentration variations with cell depth, are presented in Fig. 8(a)–(b). As the reverse voltage escalates, the concentration of electrons diminishes

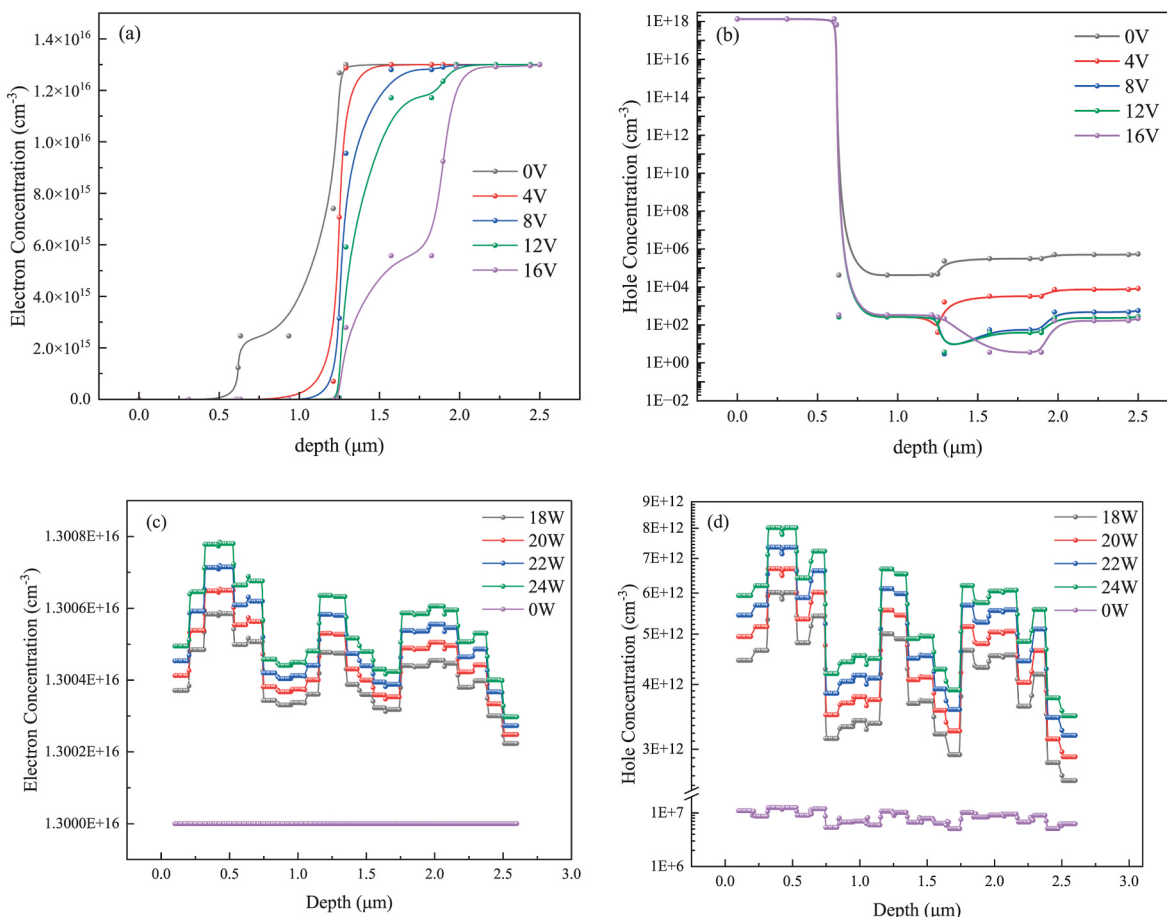


**Fig. 8.** Electron and hole concentration under different LECO process parameters: (a) electron concentration under different reverse voltage without laser; (b) hole concentration under different reverse voltage without laser; (c) electron concentration under different laser power without reverse voltage; (d) hole concentration under different laser power without reverse voltage.

within the depth range of 0.6–2  $\mu\text{m}$ . Beyond a depth of 2  $\mu\text{m}$ , the electron concentration returns to its standard level (Fig. 8(a)). In a similar manner, the concentration of holes is maintained at standard levels to a depth of 0.6  $\mu\text{m}$  (see Fig. 8(b)). However, when a reverse voltage is applied, the hole concentration decreases with increasing voltage, exhibiting a two-order-of-magnitude difference compared to the case without reverse voltage. The observed changes in electron and hole concentrations, combined with Figs. S2 and S3 in the Supplementary Material, demonstrate that reverse voltage induces movement of both electrons and holes.

The findings regarding the varying concentrations of electrons and holes, which are predominantly situated within the 0–2.5  $\mu\text{m}$  range on the anterior surface, have been illustrated in Fig. 8(c)–(d). Fig. 8(d) shows the hole concentration in phosphorus-doped wafers. Initially, without laser treatment, the hole concentration is  $1 \times 10^7 \text{ cm}^{-3}$ . However, the hole concentration increases significantly after laser treatment, reaching a peak of  $8 \times 10^{12} \text{ cm}^{-3}$ . The changes in electron and hole concentrations following laser treatment exhibit similar trends. This observation, combined with supplementary materials in Figs. S4 and S5, indicates that the electron concentration increases linearly with the rise in laser power.

#### 4. Conclusions

This study systematically analyzes the influence of various process parameters on the LECO process. Initially, the influence of the sintering temperature was assessed, thereby highlighting its substantial effect on glass corrosion, which has the potential to undermine the passivation

layer. Optimal cell efficiency was achieved at a peak sintering temperature of approximately 790 °C. Reducing the sintering temperature further resulted in decreased glass corrosion, accompanied by a 0.2 % reduction in FF and an increase in  $\rho_c$  of 0.9  $\text{m}\Omega \text{ cm}^2$ . Conversely, higher sintering temperatures intensified glass corrosion, leading to a rapid increase in  $J_{0,\text{metal}}$ , from 182  $\text{fA/cm}^2$  to 256  $\text{fA/cm}^2$ . The results also highlighted the role of reverse voltage in directing charge carrier movement. Once a threshold voltage is reached, further adjustments have minimal effect on contact formation. However, insufficient reverse voltage fails to guide carriers effectively, reducing FF by approximately 0.1 %. In contrast, variations in reverse voltage had negligible effects on  $V_{oc}$  and  $J_{sc}$ , as reverse voltage primarily influences current magnitude during the LECO process, significantly impacting contact quality. Laser treatment enhanced the minority carrier lifetime without damaging the passivation layer. Increasing laser power during the LECO process improved contact optimization, though excessive power generated surplus carriers and reverse currents, potentially damaging the passivation layer. Hence, precise laser power is crucial to ensure effective current formation without adverse effects.

COMSOL simulations further clarified the roles of reverse voltage and laser treatment in the LECO process. Reverse voltage facilitated the separation of electrons and holes, while laser treatment generated excess charge carriers that promoted current formation. The findings confirm the significant impact of LECO parameters on the I-V performance of TOPCon cells. Future optimizations should consider various cell structures to facilitate improved contact formation and enhanced device efficiency.

## CRediT authorship contribution statement

**Qinqin Wang:** Writing – review & editing, Writing – original draft, Supervision, Software, Resources, Methodology, Investigation, Formal analysis, Data curation. **Kaiyuan Guo:** Writing – review & editing, Software, Methodology, Investigation, Formal analysis. **Siwen Gu:** Writing – review & editing, Investigation, Formal analysis. **Wangping Wu:** Writing – review & editing. **Lvzhou Li:** Writing – review & editing, Resources. **Deniz Eren Erişen:** Writing – review & editing. **Gao Yong:** Resources, Investigation. **Jianning Ding:** Writing – review & editing, Resources.

## Declaration of competing interest

The authors declare that they have no known competing financial interests or personal relationships that could have appeared to influence the work reported in this paper.

## Acknowledgment

This work has been partially supported by the National Key Research and Development Program of China (2023YFB4202604) and the National Natural Science Foundation of China (No. 62304199).

## Appendix A. Supplementary data

Supplementary data to this article can be found online at <https://doi.org/10.1016/j.solmat.2025.113526>.

## Data availability

Data will be made available on request.

## References

- [1] W.H. Chen, R.Z. Liu, Q.G. Zeng, L. Zhou, Low cost multicrystalline bifacial PERC solar cells - fabrication and thermal improvement, *Sol. Energy* 184 (2019) 508–514.
- [2] J. Schmidt, R. Peibst, R. Brendel, Surface passivation of crystalline silicon solar cells: present and future, *Sol. Energy Mater. Sol. Cells* 187 (2018) 39–54.
- [3] S.P. Padi, M.Q. Khokhar, S. Chowdhury, E.C. Cho, J. Yi, Nanoscale SiO<sub>x</sub> tunnel oxide deposition techniques and their influence on cell parameters of TOPCon solar cells, *Trans. Electr. Electron. Mater.* 22 (2021) 557–566.
- [4] D. Yan, A. Cuevas, J.I. Michel, C. Zhang, Y.M. Wan, X.Y. Zhang, J. Bullock, Polysilicon passivated junctions: the next technology for silicon solar cells? *Joule* 5 (2021) 811–828.
- [5] D. Yan, A. Cuevas, S.P. Phang, Y.M. Wan, D. Macdonald, 23% efficient p-type crystalline silicon solar cells with hole-selective passivating contacts based on physical vapor deposition of doped silicon films, *Appl. Phys. Lett.* 113 (2018) 4.
- [6] M.K. Stodolny, M. Lenes, Y. Wu, G.J.M. Janssen, I.G. Romijn, J.R.M. Luchies, L. J. Geerligs, n-Type polysilicon passivating contact for industrial bifacial n-type solar cells, *Sol. Energy Mater. Sol. Cells* 158 (2016) 24–28.
- [7] T. Gao, Q. Yang, X.Q. Guo, Y.Q. Huang, Z. Zhang, Z.X. Wang, M.D. Liao, C.H. Shou, Y.H. Zeng, B.J. Yan, G.F. Hou, X.D. Zhang, Y. Zhao, J.C. Ye, An industrially viable TOPCon structure with both ultra-thin SiO<sub>x</sub> and n<sup>+</sup> poly-Si processed by PECVD for p-type c-Si solar cells, *Sol. Energy Mater. Sol. Cells* 200 (2019) 8.
- [8] J.S. Chiu, Y.M. Zhao, S. Zhang, D.S. Wu, The role of laser ablated backside contact pattern in efficiency improvement of mono crystalline silicon PERC solar cells, *Sol. Energy* 196 (2020) 462–467.
- [9] Q.Q. Wang, S.W. Gu, K.Y. Guo, H. Peng, W.P. Wu, J.N. Ding, Influence of the medium-temperature light soaking process on the passivation and electronic performance of the N-TOPCon solar cells, *Sol. Energy Mater. Sol. Cells* 273 (2024) 14.
- [10] D. Ding, Z.R. Du, R.L. Liu, C. Quan, J. Bao, D.X. Du, Z.P. Li, J. Chen, W.Z. Shen, Laser doping selective emitter with thin borosilicate glass layer for n-type TOPCon c-Si solar cells, *Sol. Energy Mater. Sol. Cells* 253 (2023) 9.
- [11] A. Richter, J. Benick, F. Feldmann, A. Fell, M. Hermle, S.W. Glunz, n-Type Si solar cells with passivating electron contact: identifying sources for efficiency limitations by wafer thickness and resistivity variation, *Sol. Energy Mater. Sol. Cells* 173 (2017) 96–105.
- [12] Q.Q. Wang, H. Peng, S.W. Gu, K.Y. Guo, W.P. Wu, B.R. Li, L.Z. Li, N.Y. Yuan, J. N. Ding, High-efficiency n-TOPCon bifacial solar cells with selective poly-Si based passivating contacts, *Sol. Energy Mater. Sol. Cells* 259 (2023) 13.
- [13] Z.B. Liu, C.L. Guo, Y. Liu, J.H. Wang, X.P. Su, Q.Q. Wang, Performance of large area n-TOPCon solar cells with selective poly-Si based passivating contacts prepared by PECVD method, *Materials* 17 (2024) 21.
- [14] Q.Q. Wang, K.Y. Guo, L. Yuan, L. Li, H. Peng, B.R. Li, A.L. Wang, L.Z. Zhang, W. P. Wu, J.N. Ding, N.Y. Yuan, Boron tube diffusion process parameters for high-efficiency n-TOPCon solar cells with selective boron emitters, *Sol. Energy Mater. Sol. Cells* 253 (2023) 11.
- [15] X.D. Xu, W.P. Wu, Q.Q. Wang, Efficiency improvement of industrial silicon solar cells by the POCl<sub>3</sub> diffusion process, *Materials* 16 (2023) 9.
- [16] H.Y. Xing, Z.K. Liu, Z.H. Yang, M.D. Liao, Q.Q. Wu, N. Lin, W. Liu, C.F. Ding, Y. H. Zeng, B.J. Yan, J.C. Ye, Plasma treatment for chemical SiOx enables excellent passivation of p-type polysilicon passivating contact featuring the lowest J<sub>0</sub> of 6 fA/cm<sup>2</sup>, *Sol. Energy Mater. Sol. Cells* 257 (2023) 10.
- [17] D. Ma, W. Liu, M.J. Xiao, Z.H. Yang, Z.K. Liu, M.D. Liao, Q.L. Han, H. Cheng, H. Y. Xing, Z.T. Ding, B.J. Yan, Y.D. Wang, Y.H. Zeng, J.C. Ye, Highly improved passivation of PECVD p-type TOPCon by suppressing plasma-oxidation ion-bombardment-induced damages, *Sol. Energy* 242 (2022) 1–9.
- [18] N. Lin, Z.H. Yang, H.J. Du, Z.T. Ding, Z.K. Liu, H.Y. Xing, M.J. Xiao, Y.L. Ou, W. Liu, M.D. Liao, B.J. Yan, S.H. Huang, Y.H. Zeng, J.C. Ye, Excellent surface passivation of p-type TOPCon enabled by ozone-gas oxidation with a single-sided saturation current density of ~ 4.5 fA/cm<sup>2</sup>, *Sol. Energy* 259 (2023) 348–355.
- [19] C. Madumelu, Y.L. Cai, C. Hollemann, R. Peibst, B. Hoex, B.J. Hallam, A. H. Soeriyadi, Assessing the stability of p<sup>+</sup> and n<sup>+</sup> polysilicon passivating contacts with various capping layers on p-type wafers, *Sol. Energy Mater. Sol. Cells* 253 (2023) 12.
- [20] C.L. Guo, R. Jia, X. Li, X.R. Tian, J.W. Chen, H.Y. Ge, H.W. Huang, L. Yuan, C. Xu, Influence of backside surface morphology on passivation and contact characteristics of TOPCON solar cells, *Sol. Energy* 258 (2023) 278–288.
- [21] S. Kim, J. Jeong, H. Kim, M.Q. Khokhar, S.K. Dhungel, V.A. Dao, D.P. Pham, Y. Kim, J. Yi, Bi-polysilicon passivating contact technique for crystalline silicon solar cell, *Mater. Sci. Semicond. Process.* 160 (2023) 8.
- [22] F. Feldmann, J. Schön, J. Niess, W. Lerch, M. Hermle, Studying dopant diffusion from Poly-Si passivating contacts, *Sol. Energy Mater. Sol. Cells* 200 (2019) 6.
- [23] Q.Q. Wang, K.Y. Guo, S.W. Gu, W. Huang, H. Peng, W.P. Wu, J.N. Ding, Electrical performance, loss analysis, and efficiency potential of industrial-type PERC, TOPCon, and shj solar cells: a comparative study, *Prog. Photovoltaics* 32 (2024) 889–903.
- [24] T. Fellmeth, H. Höffler, S. Mack, E. Krassowski, K. Krieg, B. Kafle, J. Greulich, Laser-enhanced contact optimization on i-TOPCon solar cells, *Prog. Photovoltaics* 30 (2022) 1393–1399.
- [25] X.Y. Wu, X.T. Wang, W.G. Yang, J.J. Nie, J. Yuan, M.U. Khan, A. Ciesla, C. Sen, Z. C. Qiao, B. Hoex, Enhancing the reliability of TOPCon technology by laser-enhanced contact firing, *Sol. Energy Mater. Sol. Cells* 271 (2024) 9.
- [26] H. Höffler, F. Simon, E. Krassowski, J. Greulich, Understanding current paths and temperature distributions during ‘laser enhanced contact optimization’ (LECO), *AIP Conf. Proc.* 2826 (2023).
- [27] S. Grosser, E. Krassowski, S. Swatek, H.M. Zhao, C. Hagendorf, Microscale contact formation by laser enhanced contact optimization, *IEEE J. Photovoltaics* 12 (2022) 26–30.
- [28] D. Ourinson, G. Emanuel, K. Rahmanpour, F. Ogiewa, H. Müller, E. Krassowski, H. Höffler, F. Clement, S.W. Glunz, Laser-powered Co-firing process for highly efficient Si solar cells, *IEEE J. Photovoltaics* 11 (2021) 282–288.
- [29] Q.Q. Wang, K.Y. Guo, S.W. Gu, W. Huang, W.P. Wu, J.N. Ding, Investigation on effects of the laser-enhanced contact optimization process with Ag paste in a boron emitter for n-TOPCon solar cell, *Prog. Photovoltaics* 33 (2024) 251–373.
- [30] Y. Fan, S. Zou, Y.L. Zeng, L.F. Dai, Z.P. Wang, Z. Lu, H. Sun, X.S. Zhou, B.C. Liao, X. D. Su, Investigation of the Ag-Si contact characteristics of boron emitters for n-tunnel oxide-passivated contact solar cells metallized by laser-assisted current injection treatment, *Sol. RRL* 8 (2024) 11.
- [31] E. Krassowski, S. Grober, M. Turek, A. Henning, H. Zhao, Investigation of monocrystalline p-type PERC cells featuring the laser enhanced contact optimization process and new LECO paste, *AIP Conf. Proc.* 2367 (2021).
- [32] M. Amarasinghe, E. Colegrave, J. Moseley, H. Moutinho, D. Albin, J. Duenow, S. Jensen, J. Kephart, W. Sampath, S. Sivananthan, M. Al-Jassim, W.K. Metzger, Obtaining large columnar CdTe grains and long lifetime on nanocrystalline CdSe, MgZnO, or CdS layers, *Adv. Energy Mater.* 8 (2018) 9.
- [33] A.X. Shang, X.F. Li, Photovoltaic devices: opto-electro-thermal physics and modeling, *Adv. Mater.* 29 (2017) 8.